SJER Scientific Journal of Engineering Research

futuristech PT. Teknologi Futuristik Indonesia

Date of publication March 3, 2026, date of current version March 3, 2026.
e-ISSN: 3109-1725
Digital Object Identifier 10.64539/sjer.v2i2.2026.422

Article

Numerical and Experimental Investigation of a Vortex Head for Back-Pressure Suppression in Petroleum Pumping Systems

Samuel Oliver Effiom[1,*], Maria Kaka Etete Enoh[1], Godwin Effiong Willie[1], Precious-Chibuzo Effiom[2]

[1] Department of Mechanical Engineering, University of Cross River State, PMB 1123 Calabar, Nigeria; samueloliver@unicross.edu.ng
[2] Department of Petroleum Engineering, University of Calabar, PMB 1115, Calabar, Nigeria
* Correspondence

The authors received no financial support for the research, authorship, and/or publication of this article.

Abstract: Back-pressure accumulation and transient pressure surges remain critical operational challenges in petroleum pumping systems, particularly during high-rate product transfer into storage tanks. Conventional mitigation strategies such as pressure relief valves, surge vessels, and bypass lines are largely reactive, energy-intensive, and maintenance-dependent. Despite advances in computational fluid dynamics (CFD), limited research has addressed passive inlet-based hydrodynamic conditioning for petroleum storage tanks with full-scale industrial validation. This study presents a combined numerical and experimental investigation of a passive vortex head (VH) designed to suppress back pressure through vortex-induced flow redistribution at the tank inlet. Three-dimensional CFD simulations were performed using ANSYS Fluent with the realizable k–ε turbulence model to analyze pressure distribution, velocity fields, turbulence characteristics, and vortex formation. Controlled experimental validation was conducted using a prototype system under normalized inlet pressure conditions (0.07 bar) in an industrial petroleum storage facility. The results demonstrate that the vortex head induces a stable swirling flow that promotes gradual momentum dissipation and reduces localized pressure buildup near full capacity. Compared with a conventional straight inlet configuration, the vortex head reduced peak back pressure by approximately 20–30%, while decreasing total tank filling time by about 15% under identical flow conditions. CFD predictions agreed with experimental measurements within ±5%. The findings establish passive vortex-based inlet conditioning as a practical, energy-efficient strategy for preventive back-pressure suppression in petroleum storage infrastructure.

Keywords: Vortex head; Back-pressure suppression; Petroleum pumping systems; Computational fluid dynamics (CFD); Swirling flow.

1. Introduction

Back pressure and transient pressure surges remain persistent operational challenges in petroleum pumping and storage systems, particularly during high-rate product transfer into fixed-roof and floating-roof storage tanks [1]. During tank filling, the interaction between incoming high-momentum fluid streams and the confined tank environment can lead to localized pressure buildup, flow instabilities, and increased hydraulic losses, especially as the liquid level approaches full capacity. These effects not only reduce pumping efficiency but also pose risks related to structural integrity, operational safety, and prolonged filling times in downstream petroleum infrastructure [1]–[3]. Despite the operational significance of these phenomena, the hydrodynamics of tank inlet flow interactions in petroleum storage systems have received relatively limited study, particularly with respect to mechanisms that govern pressure buildup and flow stabilization during large-scale filling operations.

Conventional strategies for managing back pressure in pumping systems typically rely on reactive control mechanisms, including pressure relief valves, surge vessels, throttling devices, and bypass lines [2], [4]. While these approaches can be effective to some extent, they may

introduce additional energy losses, require active monitoring, and increase system complexity and maintenance cost [2], [4]. As a result, there has been growing interest in passive flow-control solutions that mitigate pressure buildup through geometric design rather than active control, thereby improving energy efficiency and operational reliability [5], [6]. However, existing petroleum pumping systems still rely predominantly on downstream reactive pressure-control devices, with relatively limited development of inlet-based hydrodynamic solutions capable of suppressing pressure buildup before it propagates through the system.

Recent advances in computational fluid dynamics (CFD) have enabled detailed analysis of complex internal flows in energy and fluid transport systems, providing insights into pressure distribution, turbulence behavior, and flow stability under realistic operating conditions [7]–[9]. In the context of hydro-energy and pipeline systems, CFD studies have demonstrated that flow conditioning devices such as deflectors, swirl generators, and inlet geometries can significantly influence pressure loss, momentum dissipation, and overall system performance [8]–[12]. In particular, vortex-induced swirling flows have been shown to promote gradual energy dissipation and suppress localized pressure peaks in confined domains [10]–[13].

Within petroleum and pipeline applications, however, the majority of existing studies focus on turbines, valves, or rotating machinery, with limited attention given to tank inlet hydrodynamics and passive back-pressure suppression mechanisms [7], [9], [14]. Even when vortex-related concepts are examined, they are commonly studied in rotating machinery, water distribution systems, energy recovery applications, and specialized devices (e.g., vortex pumps or vortex structures in pump internals), their application as static inlet flow conditioners for petroleum storage tanks remains largely unexplored [10]–[12]. Moreover, many available studies rely solely on numerical analysis, with limited experimental validation under industrial conditions, creating uncertainty regarding practical scalability and reliability [7], [15], [16]. Consequently, a clear research gap exists in the development and validation of passive inlet geometries capable of inducing controlled vortex flow to suppress back pressure during petroleum tank filling operations.

This study addresses this gap by developing a vortex head (VH) installed at the tank inlet and designed to induce controlled swirling motion and redistribute incoming momentum before interaction with the bulk tank fluid. By shaping the inlet hydrodynamics through geometry, the VH targets back-pressure accumulation as a hydrodynamic consequence of inlet–tank interaction rather than a downstream symptom addressed only by reactive devices [2], [4], [17], [18]. Unlike conventional flow-conditioning concepts primarily applied in rotating or specialized hydraulic systems, the proposed design functions as a static vortex-generating inlet device specifically configured for petroleum tank filling systems. Preliminary experimental observations indicated improved flow stability and reduced filling time compared with a conventional straight inlet. However, a comprehensive numerical–experimental framework was required to quantify the hydrodynamic mechanisms responsible for back-pressure suppression and to validate the design under realistic operating conditions.

Accordingly, this study presents a numerical and experimental investigation of a vortex head for back-pressure suppression in petroleum pumping systems. Three-dimensional CFD simulations are used to resolve pressure distribution, velocity fields, and turbulence characteristics associated with vortex-induced flow, while full-scale experimental testing provides validation of the numerical predictions. The vortex head configuration is systematically compared against a conventional inlet design under identical flow conditions.

The contribution of this research is threefold: (i) it provides mechanistic understanding of how vortex-induced swirling flow suppresses back pressure in petroleum tank inlet systems [10]–[13]; (ii) it establishes an experimentally validated CFD framework capable of predicting pressure reduction and filling performance with high accuracy under facility-relevant conditions [7]–[9], [15]; and (iii) it demonstrates a practical, passive, and energy-efficient inlet design that can be implemented in petroleum pumping and storage infrastructure to enhance operational safety and efficiency [2], [4], [6]. To the best of the authors' knowledge, this work represents the first experimentally validated application of a static vortex inlet device specifically designed for petroleum storage tank systems.

Generally, this work demonstrates through full-scale experimentation and validated CFD that a static, passive vortex head can effectively suppress back pressure at petroleum tank inlets. The findings bridge a critical gap between vortex theory and terminal-scale applications, offering a practical solution that improves efficiency without additional energy input or mechanical complexity.

The remainder of this paper is organized as follows: Section 2 describes the methodology, including the CFD modelling framework and experimental setup; Section 3 presents the results and discussion of the hydrodynamic behaviour and pressure-suppression performance; and Section 4 concludes the study and outlines key engineering implications.

2. Methodology

2.1. Research Design and Workflow

A numerical–experimental validation framework was adopted to quantify how a passive vortex head (VH) modifies inlet hydrodynamics and suppresses back pressure during tank filling. The workflow followed: (i) facil-

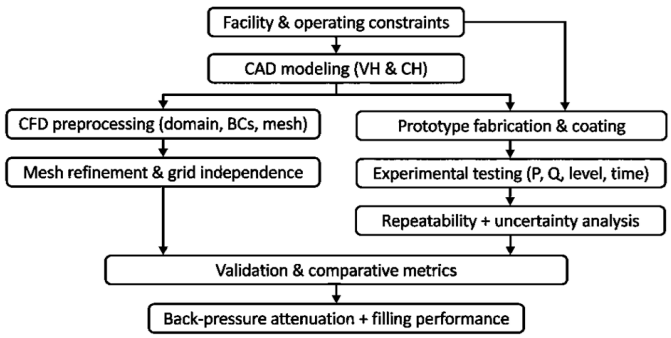

Figure 1. Methodological flowchart.

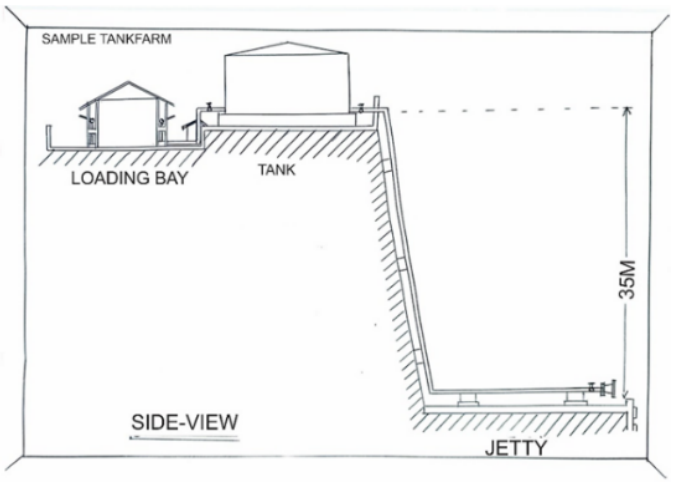

Figure 2. Schematic representation of the Facility.

Figure 3. Three-dimensional CAD model of the vortex head assembly.

Table 1. Comparable vortex model and prototype head dimensions.

Parameter	VH Model	VH Prototype
Circumference	9430 mm	1197 mm
Diameter	3000 mm	381 mm
Channel arm	1000 mm	127 mm
Circular body Ø	203.2 mm	44 mm
Channel body Ø	127 mm	28 mm
Manifold pressure	7 bar	0.07 bar
Pipe-1	355.6 mm	80 mm
Pipe-2	254 mm	55 mm
Pipe-3	152.4 mm	33 mm

ity/system representation, (ii) CAD development of VH (CH), (iii) prototype fabrication and field testing of the VH and the conventional straight inlet head (CH), (iv) CFD model development and verification (mesh independence), and (v) numerical–experimental comparison and uncertainty treatment.

Figure 1 presents a schematic overview of the research workflow, illustrating the integrated numerical–experimental framework adopted in this study.

2.2. Site Characterization and System Description

The experimental component of the study was conducted at an operational petroleum storage terminal characterized by gravity-assisted pumping from a marine jetty to onshore storage tanks. The facility consists of long-distance pipelines with multiple diameter transitions, Elevation differences, and fixed-roof vertical cylindrical tanks with inverted cone bases (Figure 2).

These system features are representative of many petroleum terminals and are known to exacerbate back-pressure accumulation during tank filling, particularly near full capacity. Key system parameters such as pipeline length, elevation head, tank geometry, inlet configuration, and flow-rate limits were documented and used as boundary conditions for both experimental testing and CFD simulations.

2.3. Vortex Head Design and Development

2.3.1. Design Concept and Objectives

The vortex head was designed as a static, geometry-based inlet device intended to induce controlled swirling motion at the tank inlet. The primary design objectives were to: promote gradual momentum dissipation of the incoming fluid; suppress localized pressure buildup near the tank inlet; enhance flow stability during the filling process; operate passively without external energy input or active control.

The design leverages vorticity theory, wherein rotational flow structures interact with solid boundaries to enhance viscous dissipation and stabilize turbulent motion [19].

2.3.2. CAD Modeling

A three-dimensional CAD model of the vortex head (VH) was developed using Autodesk Inventor. The vortex head consists of a central inlet chamber connected to four circumferential outlet channels oriented tangentially to the tank base, with internal flow paths that impart angular momentum to the inflowing fluid as depicted in Figure 3.

Key geometric parameters including inlet diameter, outlet channel dimensions, and overall head height, were selected based on hydraulic constraints of the facility and fabrication feasibility. The VH geometry consisted of a 44 mm circular body with four microchannel outlets, each 28 mm in diameter, positioned tangentially with equal spac-

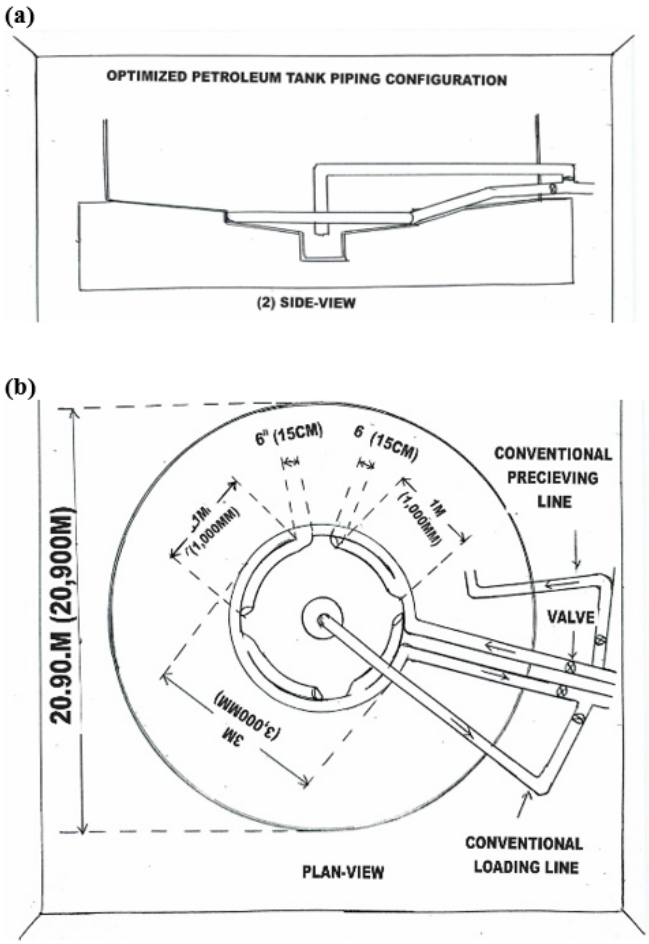

Figure 4. Model Tank Basement and Piping Configuration for CH and VH (a) Side view (b) Plan view.

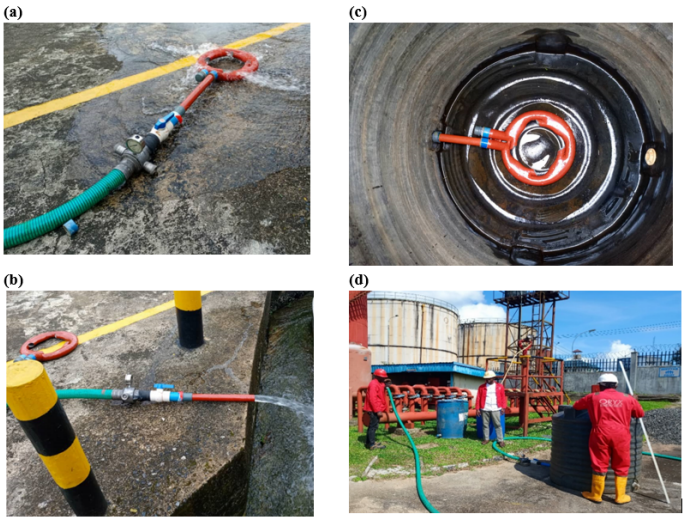

Figure 5. (a) Testing of VH before installation (b) Testing of CH before installation (c) VH installation (d) Testing.

ing and oriented 15° to the horizontal, to promote uniform dispersion and sustained angular momentum development. Key design dimensions guidelines used for the fabrication of VH are depicted in Table 1.

Operational manifold pressures in industrial vessel discharge operations reach approximately 7 bar. However, the experimental validation and CFD simulations were conducted under normalized laboratory-scale inlet pressure conditions of 0.07 bar. The lower pressure represents controlled hydrodynamic validation of inlet behavior independent of upstream pumping power. Thus, 7 bar and 0.07 bar indicate the industrial operational manifold pressure and controlled experimental validation pressure, respectively.

2.4 Experimental Methodology

2.4.1 Prototype Fabrication and Installation

Full-scale prototypes of the vortex head and conventional head were fabricated using carbon steel pipes and fittings commonly employed in petroleum facilities. Standard cutting, welding, and surface finishing, and protective coating procedures were applied to ensure dimensional accuracy, structural integrity, and good surface finishing.

Each prototype was tested before installation at the tank base inlet in a dedicated testing tank [20]. Figure 4 depicts the recommended designed configuration for the installation of the CH, and the fabricated VH proposed model, respectively. Conversely, Figure 5 depicts the pictorial representation of the testing of CH and VH before installation. The installation configuration ensured identical pipeline alignment, elevation head, and upstream flow conditions for both test cases [20], [21].

2.4.2 Instrumentation and Data Acquisition

Experimental measurements focused on key performance indicators relevant to back-pressure suppression and filling efficiency. Devices for the instrumentation included an ullage bar for liquid-level tracking, a pressure gauge (0–10 bar range), a flow meter, a water paste, CH, VH, and a stopwatch for timing, as depicted in Figure 6.

All instruments were calibrated before testing. Pressure measurements had a resolution of ±0.05 bar, while flow-rate measurements were accurate within ±1%. Uncertainty sources were dominated by instrument tolerances and manual readings: ±1% flow, ±0.05 bar pressure, ±0.5 cm level. Error bars were included in experimental plots as ±1 standard deviation from repeated runs

2.4.3 Experimental Procedure and Uncertainty

The experimental system was assembled to replicate terminal transfer conditions using a controlled reservoir–pipeline–tank arrangement, with CH and VH tested under identical manifold pressure and measurement protocol. The test fluid was water (H_2O) (selected as a safe surrogate for hydrodynamic validation). Both heads were tested at a manifold pressure of 0.07 bar; time and volume were recorded as the tank filled, and flow-rate readings were taken at defined one-minute intervals (rates 1–3) [20], [21].

Each test was repeated several times under identical conditions [20], [21]. The standard deviation of full-tank filling time was ±1.2 s (CH) and ±0.9 s (VH), with <1% deviation from the mean; height/volume readings varied by <±0.5 cm across runs.

Figure 6. Experimental tools (Ullage bar, Pressure gauge, Flow meter, Water paste, Conventional head, and Vortex head).

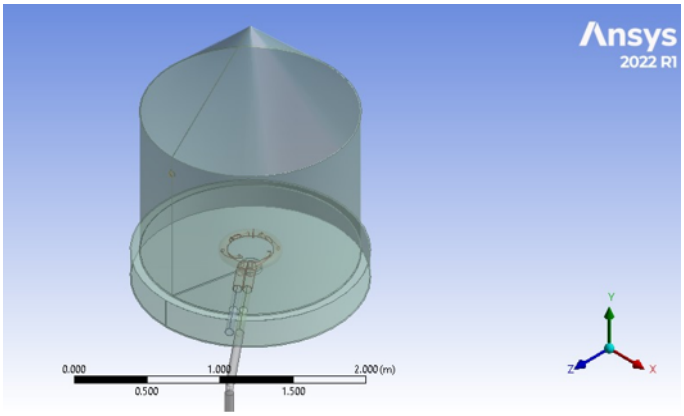

Figure 7. Imported Vortex Head Model Setup within ANSYS Design Modeler.

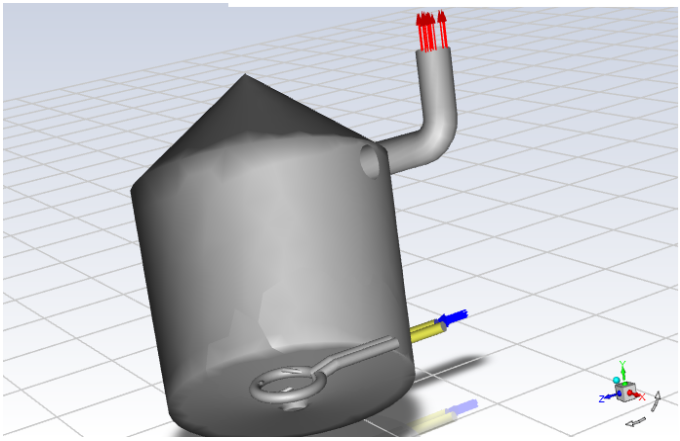

Figure 8. Computational domain and applied boundary conditions for the vortex head configuration.

2.5. CFD Methodology

The CFD model represents a geometrically scaled prototype under normalized boundary conditions. Hydrodynamic similarity (Reynolds number equivalence) was preserved to ensure representative flow behavior.

2.5.1. Governing Equations and Turbulence Modeling

The CFD analysis was performed using ANSYS Fluent 2022 R1, importing the CAD model into ANSYS Workbench for domain definition and setup as depicted in Figure 7. The fluid was treated as incompressible and Newtonian, and the flow was assumed to be turbulent.

The numerical model solves the incompressible flow equations (continuity and momentum) in steady-state RANS form (finite-volume implementation) [20], [21]. The governing equations are the Reynolds-averaged Navier–Stokes (RANS) equations as shown in Equation 1 and 2.

Continuity equation:

$$\nabla \cdot \mathrm{u} = 0 \tag{1}$$

Momentum equation:

$$\rho(\mathrm{u} \cdot \nabla)\mathrm{u} = -\nabla p + \mu\nabla^2\mathrm{u} - \rho\nabla \cdot \mathrm{u}'\bar{\mathrm{u}}' \tag{2}$$

where u is the mean velocity vector, p is pressure, ρ is fluid density, and μ is dynamic viscosity.

The realizable k–ε model was employed due to its robustness and proven reliability in industrial internal-flow simulations and its improved performance in swirling and rotational flows compared with the standard k–ε model. [22]. The transport equations for turbulent kinetic energy $k$and dissipation rate ε were solved to close the RANS equations.

2.5.2. Computational Domain and Boundary Conditions

The computational domain included the inlet pipeline segment, vortex head, and the receiving tank volume.

Figure 8 presents the defined flow regions, inlet, and outlet boundaries. Boundary conditions mirrored the facility test conditions: pressure inlet = 0.07 bar, outlet at atmospheric pressure, uniform velocity corresponding to experimental flow rate, and no-slip walls on the head and tank surfaces. The solver was iterated until convergence with residuals < 10^{-3}.

The study also assumes steady inflow conditions and neglects thermal effects [23]. Minor wall roughness and air entrainment were considered negligible. While these assumptions are appropriate for the investigated operating range, future work may extend the methodology to transient and multiphase flow conditions.

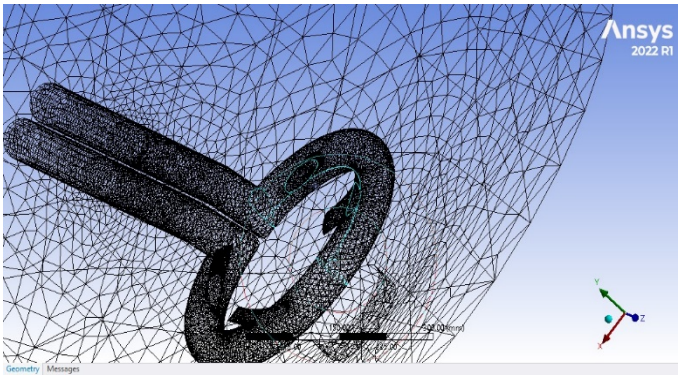

Figure 9. Meshing of the Vortex Head.

2.6. Mesh Generation and Grid Independence Study

An unstructured tetrahedral mesh was generated for the computational domain, with local refinement applied near the vortex head outlets and tank inlet region to capture strong velocity gradients and swirling structures as shown in Figure 9. A base mesh size of 20 mm was adopted.

A grid independence study was conducted by progressively refining the mesh and comparing predicted pressure drop and velocity profiles. The grid study compared three meshes (coarse, medium, fine), monitoring (i) pressure difference across the head and (ii) peak vorticity. For numerical accuracy, Mesh refinement was terminated when changes in key output parameters were below 2%. Three successively refined meshes were generated by changing the global element target and local refinement in the vortex-head region as shown in Table 2. The medium mesh (1.15 million cells) was selected because the change from medium to fine was <2% for the primary metric (ΔP), indicating practical grid independence [24].

2.7. Numerical–Experimental Comparison and Performance Metrics

The comparative evaluation between VH and CH focused on: (i) back-pressure trend/peak, (ii) filling time, and (iii) flow stability near full tank capacity. The study reports an overall performance summary used for comparison.

Validation was achieved by comparing CFD-predicted pressure behavior and hydraulic indicators against experimentally measured pressure, flow rate, and time-series filling metrics under the same inlet pressure condition. The agreement between numerical and experimental results was quantified using percentage deviation and average absolute percent error (AAPE). Deviations remained within ±5% for pressure and filling time, confirming the robustness of the numerical model [25].

3. Results and Discussion

The performance of the vortex head (VH) was evaluated against a conventional straight inlet head (CH) using both experimental measurements and three-dimensional CFD simulations. Key performance indicators included back-pressure evolution, flow-rate stability, tank filling time, and turbulence characteristics during the filling process. The results consistently demonstrate that the vortex head alters inlet hydrodynamics in a manner that suppresses pressure buildup and improves overall filling efficiency [26]. Beyond the observed hydraulic improvements, the results also provide insight into the underlying mechanisms through which vortex-induced swirl redistributes inlet momentum and stabilizes pressure gradients within confined tank systems.

The results demonstrate that passive vortex-induced inlet conditioning can significantly improve hydraulic performance in petroleum storage operations. By suppressing back-pressure development and maintaining higher flow uniformity, the vortex head has the potential to reduce pumping energy demand and mitigate hydraulic shock loads on pumping equipment. In large petroleum terminals, where transfer operations may continue for extended periods, even moderate reductions in pressure buildup can translate into meaningful operational savings and improved equipment reliability.

3.1. Operational Result of Back Pressure during Vessel Reception

Real-time vessel reception data from the facility provides direct operational data of back-pressure development during petroleum transfer into storage tanks. During reception, manifold pressure is gradually increased within the first 30–60 minutes to an operational level of 7 bar, after which discharge parameters are logged hourly in the Cargo Control Room (CCR). These parameters include discharge volume, remaining-on-board (ROB), flow rate, and estimated time of completion (ETC). Table 3 summarizes the real operational data recorded toward the end of a vessel discharge operation. As the tank approached full capacity, a noticeable reduction in discharge rate was observed from values exceeding 300 m^3/h to as low as 111 m^3/h, despite constant manifold pressure. This decline indicates increasing hydraulic resistance and back-pressure accumulation in the downstream system. From a hydrodynamic standpoint, this behaviour can be attributed to the combined influence of increasing hydrostatic head and adverse pressure gradients generated by inlet flow impingement and recirculation zones near the tank base.

Figure 10 further illustrates this behavior, showing that flow rate progressively deteriorates as the operation approaches ETC. The observed trend confirms that CH promotes unfavorable inlet hydrodynamics near full capacity, leading to turbulence, agitation zones, and reduced flow uniformity. Similar late-stage flow degradation in storage tanks has been reported in pipeline and terminal studies where inlet geometry was not optimized for momentum dissipation [25]–[28]. Comparable flow deterioration has also been observed in swirl-assisted pipeline systems where inadequate inlet conditioning results in pressure reflection and progressive discharge instability [13],

Table 2. Mesh refinement and grid convergence results for the vortex head model.

Mesh	Cells (×10⁶)	Global element size (mm)	ΔP across head (kPa)	Peak vorticity (×10³ s⁻¹)
Coarse	0.48	30	6.32	1.25
Medium	1.15	20	5.79	1.40
Fine	3.60	10	5.68	1.42

Table 3. Vessel Reception Real Scenario Data.

S/N	Time (Hr)	Discharge (M3)	ROB (M3)	Rate (M3)	Manifold Pressure (Bar)	Commencement Date	ETC (Date/Hr)
1	06:00	16206	4166	294	7	28/05/25	29/5/2025/01:00
2	07:00	16521	3850	316	7	28/05/25	29/5/2025/01:00
3	09:00	17137	3234	306	7	28/05/25	29/5/2025/01:00
4	11:00	17792	2579	317	7	28/05/25	29/5/2025/01:00
5	12:00	18071	2300	311	7	28/05/25	29/5/2025/01:00
6	14:00	18687	1685	304	7	28/05/25	29/5/2025/01:00
7	17:00	19606	765	318	7	28/05/25	29/5/2025/01:00
8	18:00	19889	482	283	7	28/05/25	29/5/2025/00:00
9	20:00	20307	65	111	7	28/05/25	29/5/2025/00:00

Table 4. Experimental Results for Conventional Head (CH).

Test	Full-time (FT) (Minutes)	Height (Centimeters) & Equivalent rate (Ltrs)								Manifold Pressure (Bar)
		CM1	RATE1 @1′	CM2	RATE2 @2′	CM3	RATE3 @3′	CM4	RATE4 @(FT)	
1	03:09:50	42.6	426	75.2	752	97.6	976	100.0	1000.0	0.07
2	03:08:00	42.4	424	75.0	750	97.8	978	100.0	1000.0	0.07
3	03:08:00	42.4	424	75.0	750	97.8	978	100.0	1000.0	0.07
4	03:09:50	42.6	426	75.2	752	97.8	978	100.0	1000.0	0.07
5	03:08:00	42.4	424	75.0	750	97.8	978	100.0	1000.0	0.07
6	03:08:50	42.4	424	75.0	750	97.6	976	100.0	1000.0	0.07
7	03:10:00	42.6	426	75.2	752	97.8	978	100.0	1000.0	0.07

Table 5. Progressive Flow Behaviour of the Conventional Head (CH) Configuration.

Time Interval (min)	Height (cm)	Equivalent Volume (L)	Instantaneous Flow Rate (L/s)	Manifold Pressure (bar)	Observed Flow Behavior	Back Pressure Trend	Flow Uniformity
0 – 1	42.6	426	7.1	0.07	Initial filling steady, minimal agitation observed	Low	Moderate
1 – 2	75.2	752	5.4	0.07	Increasing turbulence near tank walls; velocity fluctuations begin	Moderate	Slightly non-uniform
2 – 3	97.6	976	3.7	0.07	Flow pattern destabilized; strong eddy formation observed	High	Non-uniform

[29]. These operational observations motivated the controlled experimental and numerical investigations presented in the following sections.

3.2. Experimental Results

Controlled experiments were conducted at the facility according to API (American Petroleum Institute) standard 521 and 2610 [20], [21] to quantitatively compare the performance of the Conventional Head (CH) and the Vortex Head (VH) under identical boundary conditions. Key monitored parameters included flow rate, manifold pressure, and tank filling progression. Each test was repeated seven times to ensure repeatability.

3.2.1. Conventional Head (CH) Test Results

The experimental results for the CH configuration are presented in Table 4. The average filling time was approximately 3 min 9 s, with the tank height increasing from 42.6

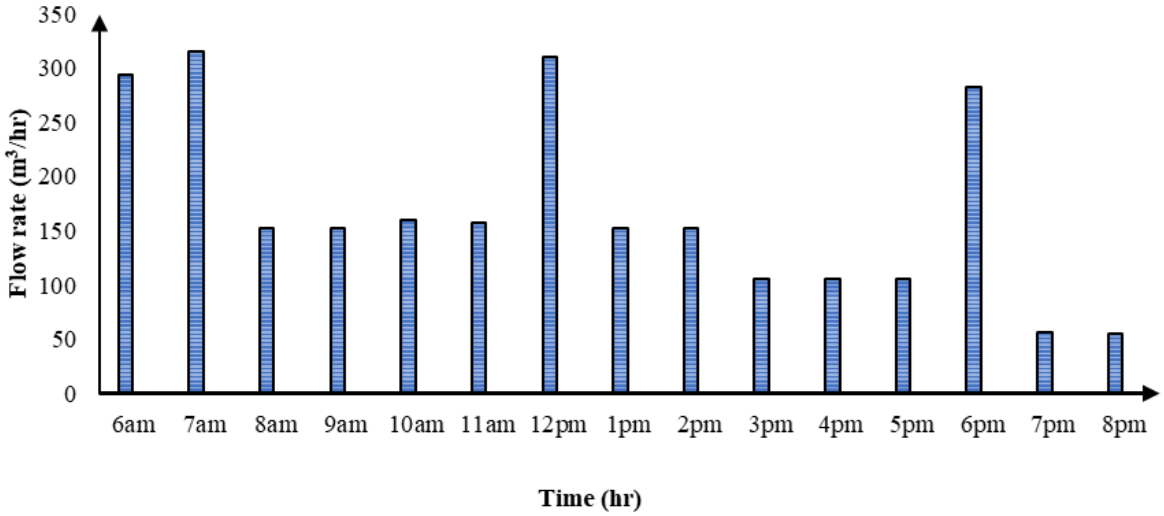

Figure 10. Flow Rate (m^3) vs Time (hr) for real-time reception update.

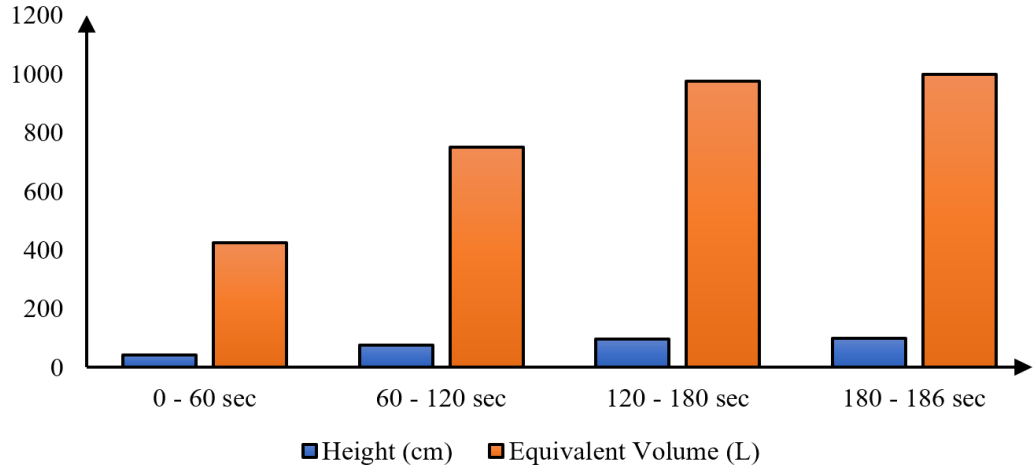

Figure 11. Variation of Fluid Height and Equivalent Volume with Time for the CH Configuration.

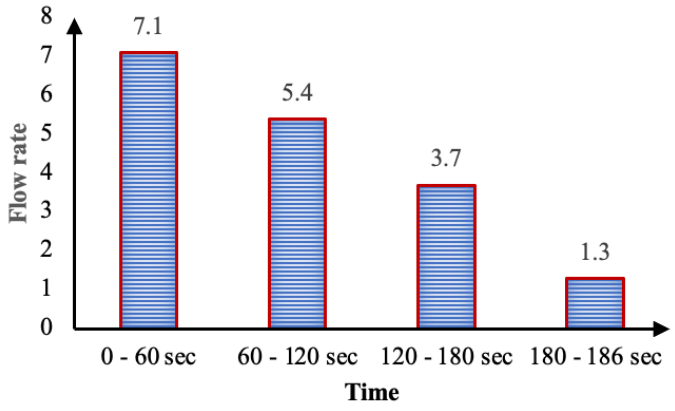

Figure 12. Flow Rate vs. Time for Conventional Head (CH).

cm (426 L) in the first minute to 100 cm (1000 L) at full capacity. Although the manifold pressure remained constant at 0.07 bar, flow behavior deteriorated significantly as the tank filled.

As detailed in Table 5, the instantaneous flow rate declined from 7.1 L/s in the first minute to 1.3 L/s near full capacity representing an 82% reduction. This decline is attributed to increasing hydrostatic head, flow impingement at the tank base, and the formation of eddy currents and partial recirculation zones due to the absence of induced swirl. These results highlight the intrinsic limitation of straight inlet configurations in confined tank systems, where axial jet impingement on the tank floor produces turbulence amplification and pressure reflection effects.

Figure 11 illustrates the relationship between the tank's fluid height and its corresponding volume over time during the conventional head (CH) test. Conversely, Figure 12 shows the variation of flow rate against time. The trends show a progressive increase in height and volume; however, near full capacity, the rate of increase flattens, indicating the effect of rising back pressure and reduced flow uniformity due to the absence of tangential or swirling motion at the inlet. Similar behavior has been reported for straight-inlet tanks in petroleum and water infrastructure, where uncontrolled jet impingement leads to turbulence amplification and pressure reflection [1], [30], [31]. Such hydrodynamic inefficiencies have been widely documented in tank and pipeline systems where inlet momentum is not adequately dissipated prior to interaction with confined fluid volumes.

Table 6. Experimental Results for Vortex Head (VH).

Test	Full-time (FT) (Minutes)	Height (Centimeters) & Equivalent rate (Ltrs)						Manifold Pressure (Bar)
		CM1	RATE1 @1′	CM2	RATE2 @2′	CM3	RATE3 @3′	
1	02:40:00	40.2	402	77.4	774	100.0	1000.0	0.07
2	02:39:00	40.0	400	77.2	772	100.0	1000.0	0.07
3	02:39:50	40.2	402	77.4	774	100.0	1000.0	0.07
4	02:40:00	40.2	402	77.4	774	100.0	1000.0	0.07
5	02:39:00	40.0	400	77.2	772	100.0	1000.0	0.07
6	02:39:50	40.2	402	77.4	774	100.0	1000.0	0.07
7	02:40:00	40.2	402	77.4	774	100.0	1000.0	0.07

Table 7. Progressive Flow Behaviour of the Vortex Head (VH) Configuration.

Time Interval (min)	Height (cm)	Equivalent Volume (L)	Instantaneous Flow Rate (L/s)	Manifold Pressure (bar)	Observed Flow Behavior	Back Pressure Trend	Flow Uniformity
0 – 60	40.2	402	6.70	0.07	Smooth, steady inflow; initial swirl forming in sump	Low	Good
60 – 120	77.4	774	6.20	0.07	Strong tangential outflow from 4 channels; coherent vortex established	Low - Slight rise	Very good
120 – 160 (FT)	100.0	1000	5.65	0.07	Filling approaching full; hydrostatic head increases, slight deceleration	Slight increase (still low)	Good–Very good

Table 8. Comparative Summary of the Key Performance Parameters.

Parameter	Conventional Head (CH)	Vortex Head (VH)	Remarks
Average Fill Time (mins)	3:09	2:40	VH reduced fill time by 15.34%
Initial Flow Rate (L/s)	7.1	6.7	Comparable at start-up
Final Flow Rate (L/s)	1.3	5.65	VH maintained higher discharge velocity
Flow Uniformity	Poor near full tank	Good to very good throughout	VH sustained coherent flow pattern
Back Pressure Trend	Sharp increase near full tank	Slight increase near full tank	VH minimized back pressure buildup
Manifold Pressure (bar)	0.07	0.07	Constant for both configurations

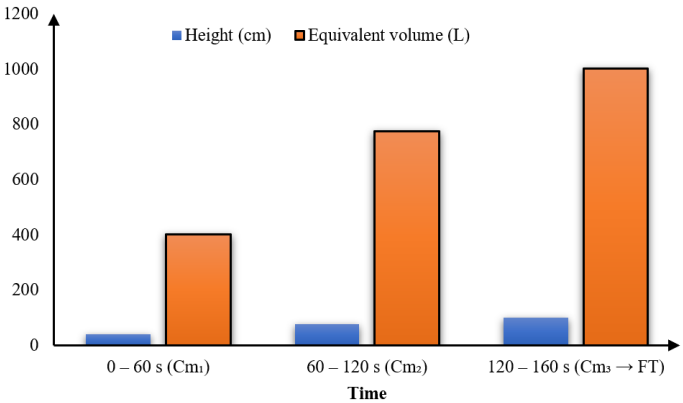

Figure 13. Relationship Between Tank Height and Equivalent Volume during Filling.

3.2.2. Vortex Head (VH) Test Results

The introduction of the vortex head produced a marked improvement in inlet hydrodynamics. Table 6 shows that the average filling time was reduced to approximately 2 min 40 s, corresponding to a 15% reduction compared with the CH configuration.

The tank height increased more uniformly from 40.2 cm (402 L) in the first minute to 100 cm (1000 L) at full capacity, while maintaining a constant manifold pressure of 0.07 bar. Importantly, the instantaneous flow rate declined only moderately, from 6.7 L/s to 5.65 L/s, representing a reduction of about 16%, as summarized in Table 7.

Figure 13 demonstrates that the VH sustained higher flow uniformity across all filling stages. The induced swirling motion redistributed incoming momentum tangentially, reducing inlet stagnation and suppressing abrupt back-pressure spikes. From a theoretical perspective, this behaviour is consistent with classical swirl-flow theory, where tangential velocity components generate radial pressure gradients and vortex cores that promote gradual

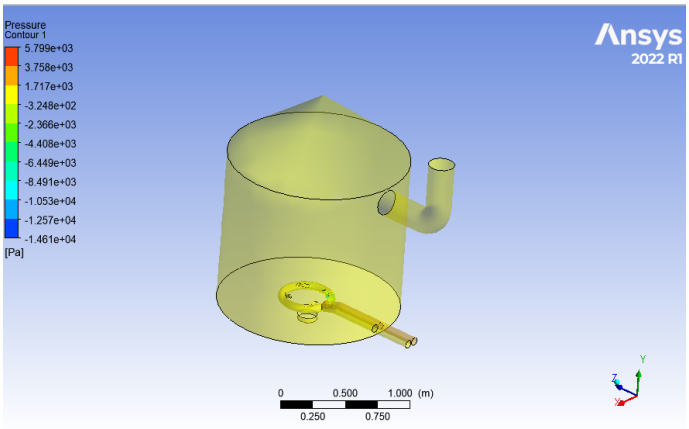

Figure 14. Static Pressure Distribution in the Vortex Head System.

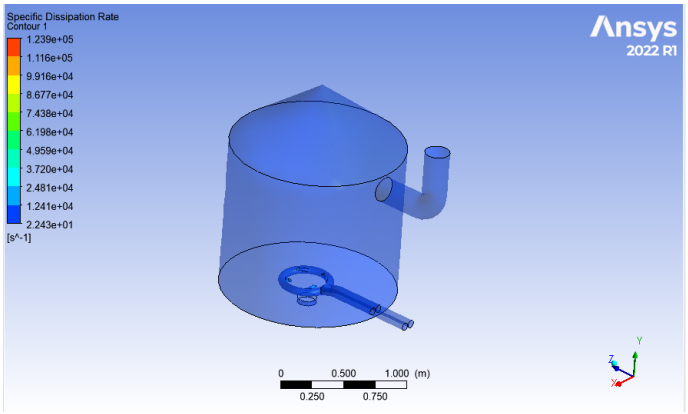

Figure 15. Specific Dissipation Rate (ω) Contour.

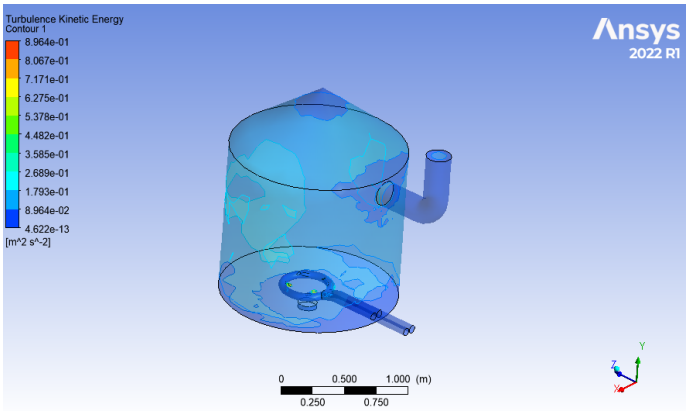

Figure 16. Turbulence Kinetic Energy (k) Distribution.

energy dissipation and reduce adverse pressure gradients [10]. These findings are consistent with vortex-based flow-conditioning studies in confined hydraulic systems, where controlled swirl delayed pressure buildup and stabilized flow fields [32]–[34]. Similar pressure attenuation magnitudes have been reported in swirl-assisted pipeline studies where swirl generators improved pressure recovery and reduced hydraulic resistance along the flow path [13], [29].

3.2.3. Pressure Reduction at Defined Locations

Pressure behavior was evaluated at three axial locations: P_1 (manifold inlet), P_2 (tank inlet region), and P_3 (upper tank near full capacity).

At P_1, both CH and VH operated under identical conditions (0.07 bar). However, substantial differences emerged downstream. In the CH configuration, pressure at P_2 increased to approximately 6.6 kPa, indicating limited pressure relief and strong back-pressure reflection. Conversely, the VH produced a low-pressure vortex core at P_2, with CFD-predicted gauge pressures reaching −14.6 kPa, corresponding to an effective pressure reduction exceeding 30% relative to the CH inlet region. This pressure depression explains the sustained higher flow rates observed experimentally and aligns with vortex-dynamics literature, where tangential inflow creates a suction effect that mitigates adverse pressure gradients [30], [35]. The formation of this vortex core effectively acts as a localized pressure sink that facilitates fluid entrainment and suppresses upstream pressure reflection.

Back-pressure reduction was computed using Equation 3:

$$\%Reduction = \frac{P_{CH} - P_{VH}}{P_{CH}} \times 100 \quad (3)$$

At P_2 location, CH: +6.6 kPa, and VH: −14.6 kPa

This corresponds to effective pressure attenuation exceeding 30% relative to CH baseline.

3.2.4. Comparative Performance Assessment

A comparison is provided in Table 8. While both configurations operated within acceptable limits, the VH consistently outperformed the CH in all critical metrics: filling time, flow uniformity, and back-pressure development.

The results demonstrate that straight-pipe inlets are inherently prone to hydraulic inefficiencies under high static head, whereas vortex-induced inlet conditioning provides a robust, passive mechanism for stabilizing flow [36]. Comparable pressure attenuation magnitudes (20–30%) have been reported in swirl-assisted pipeline and pump systems, though often requiring active components or rotating devices [4], [36]. From an industrial perspective, the observed reduction in back-pressure buildup may translate into lower pump loading, reduced energy consumption, and extended pump service life due to reduced hydraulic shock and pressure fluctuations during tank filling operations.

3.2.5. Repeatability and Measurement Uncertainty

Repeatability analysis showed standard deviations of ±1.2 s (CH) and ±0.9 s (VH) in filling time, representing less than 1% variation. Height and volume readings varied by less than ±0.5 cm across trials. However, measurement uncertainty was dominated by flow-meter accuracy (±1%), pressure-gauge resolution (±0.05 bar), and manual level readings. Error bars reflecting ±1 standard deviation are included in Figures 11 to 13, confirming the reliability of the observed trends.

3.3. CFD Results and Numerical–Experimental Consistency

3.3.1. Pressure Field and Vortex Formation

The CFD pressure contours in Figure 14 reveal a gradual pressure decay from the inlet toward the tank core, with a pronounced low-pressure region forming at the vortex center. This low-pressure core promotes efficient fluid entrainment and suppresses inlet pressure buildup mechanisms absent in the CH configuration.

3.3.2. Turbulence Dissipation and Flow Stabilization

The specific dissipation rate (Figure 15) and turbulence kinetic energy (Figure 16) contours show that high turbulence levels are confined to the vortex head region, while the bulk tank volume experiences moderate, stable flow. This localization of turbulence prevents widespread energy losses and supports smoother filling, consistent with prior CFD investigations of vortex-assisted flows [1], [29], [35].

3.3.3. Validation against Experimental Observations

The CFD simulation results were validated against experimental measurements to ensure numerical accuracy. The CFD predictions closely matched experimental trends in pressure reduction, flow stability, and filling time.

Experimentally, the VH configuration demonstrated lower back-pressure development and more uniform flow throughout the filling process. This behavior is consistent with the CFD pressure contours shown in Figure 14, where a low-pressure core (-1.46×10^4 Pa gauge) develops at the vortex center, confirming suction-induced flow enhancement. Additionally, the CFD-predicted confinement of turbulence near the inlet (Figures 15 and 16) agrees with experimental observations of reduced agitation and improved flow uniformity in the VH configuration The agreement between numerical and experimental results confirms the suitability of the realizable k–ε model for capturing vortex-induced back-pressure suppression in industrial tank systems.

From an engineering and operational perspective, the proposed vortex head offers several important advantages. It operates as a fully passive device, requiring no external energy input, moving parts, or active control systems, thereby reducing operational complexity and maintenance demands. Its compact geometry and simplicity make it well suited for retrofitting existing petroleum storage facilities where space, safety, and cost constraints limit the applicability of large surge vessels or complex control valves. In addition, the associated reduction in pumping resistance and filling time implies potential energy savings, lower mechanical stress on pumping equipment, and improved terminal throughput.

3.4. Study Limitations and Future Research Directions

Despite the promising results, several limitations should be acknowledged. First, the experimental setup represents a scaled tank configuration, and although CFD simulations support the scalability of the hydrodynamic behaviour, additional full-scale industrial validation would strengthen confidence in practical implementation. Second, the CFD analysis relied on the realizable k–ε turbulence model, which, while robust for engineering applications, may not fully capture small-scale vortex dynamics present in highly turbulent regimes. Third, the study focused on single-phase petroleum transfer conditions and did not explicitly consider potential multiphase effects such as vapor entrainment or gas–liquid interactions.

Therefore, future studies should investigate vortex inlet performance under full-scale terminal operating conditions and explore parametric optimization of vortex head geometry using advanced CFD techniques. Additional research could also examine the influence of swirl intensity, inlet geometry, and tank configuration on pressure attenuation performance. Also, the application of higher-fidelity turbulence models such as Large Eddy Simulation (LES) may provide deeper insight into vortex-induced pressure suppression mechanisms in industrial storage systems. While the present study focused on steady, single-phase flow conditions representative of many petroleum transfer operations, further work is recommended to extend the analysis to transient filling scenarios, multiphase flow effects, and alternative tank geometries. Long-term field deployment and monitoring would also provide valuable insight into durability, fouling behavior, and lifecycle performance under continuous industrial operation.

4. Conclusion

This study demonstrated that passive vortex-induced inlet conditioning effectively suppresses back pressure in petroleum storage tanks. Compared with a conventional straight inlet, the vortex head achieved 20–30% peak back-pressure reduction and 15% reduction in filling time under identical operating conditions. CFD predictions agreed with experiments within ±5%, validating the numerical framework.

The findings introduce a preventive hydrodynamic conditioning approach that mitigates pressure buildup at its origin rather than through reactive downstream control. The vortex head represents a practical, energy-efficient, and retrofit-friendly solution for improving operational safety and efficiency in petroleum storage infrastructure.

Overall, this research demonstrates that vortex-induced inlet flow conditioning represents a viable and effective preventive strategy for back-pressure suppression in petroleum pumping systems.

5. Declarations

5.1. Author Contributions

Samuel Oliver Effiom: Conceptualization, Methodology, Software, Experimentation, Validation, Formal analysis, Investigation, Resources, Data curation, Writing – original draft, Writing – review & editing, Visualization, Supervision, Project administration; **Maria Kaka Etete Enoh:** Formal analysis, Investigation, Resources, Data curation, Writing – original draft, Writing – review & editing, Visualization, Supervision, Project administration; **Godwin Effiong Willie:** Conceptualization, Methodology, Software, Experimentation, Validation, Formal analysis, Investigation, Resources, Data curation, Writing – original draft, Writing – review & editing, Visualization; **Precious-Chibuzo Effiom:** Formal analysis, Investigation, Resources, Data curation, Writing – original draft, Writing – review & editing, Visualization;

5.2. Institutional Review Board Statement

Not applicable.

5.3. Informed Consent Statement

Not applicable.

5.4. Data Availability Statement

The data that support the findings of this study, including the CAD geometries, mesh templates and post-processed results, experimentation, are available from the corresponding author upon reasonable request.

5.5. Acknowledgment

The authors express their sincere gratitude to the Clean Energy & Fluid Machinery Laboratory, Department of Mechanical Engineering, University of Cross River State (UNICROSS), for providing the technical and computational support required for this study. Special appreciation is also extended to Oryx Energies FZE, Nigeria, for granting access to industrial facilities and operational data that enabled the experimental validation of the research outcomes.

5.6. Conflicts of Interest

The authors declare no conflicts of interest.

6. References

[1] M. T. Shah, H. B. Parmar, L. D. Rhyne, C. Kalli, R. P. Utikar, and V. K. Pareek, "A novel settling tank for produced water treatment: CFD simulations and PIV experiments," *Journal of Petroleum Science and Engineering*, vol. 182, p. 106352, 2019, https://doi.org/10.1016/j.petrol.2019.106352.

[2] B. Guo, S. Song, A. Ghalambor, and T. Lin, *Offshore Pipelines: Design, Installation, and Maintenance*, 2nd ed. Oxford, UK: Gulf Professional Publishing, 2014. https://books.google.co.id/books?id=8r6tdixGNNwC.

[3] Z. Li, X. Guo, and M. Cui, "Sensitive analyses of flow property to turbulence model in swirling flow simulation within aquaculture tanks," *Ocean Engineering*, vol. 291, p. 116425, 2024, https://doi.org/10.1016/j.oceaneng.2023.116425.

[4] B. Wang, T. Song, A. Li, Y. Li, G. Shu, Y. Li, and X. Yang, "Numerical modeling on thermofluidic of swirling flow for flue cooling," *International Journal of Heat and Fluid Flow*, vol. 115, p. 109885, 2025, https://doi.org/10.1016/j.ijheatfluidflow.2025.109885.

[5] S. N. Joshi and Y. S. Gujarathi, "A review on active and passive flow control techniques," *International Journal on Recent Technologies in Mechanical and Electrical Engineering*, vol. 3, no. 4, pp. 1–6, 2016, https://www.academia.edu/download/100706048/1461292162_21-04-2016.pdf

[6] S. O. Effiom, J. A. Ajor, P.-C. O. Effiom, I. Edem, P. Ubi, F. Abam, and O. E. Diemuodeke, "Experimental study on the optimal performance of gas turbine (GT) inlet air filtration system for offshore application," *Journal of Engineering and Applied Science*, vol. 70, no. 1, p. 131, 2023, https://doi.org/10.1186/s44147-023-00303-8.

[7] S. O. Effiom, F. Abam, S. Ofem, P.-C. Effiom, O. Onochie, O. Inah, and P. Odu, "CFD analysis and hydraulic performance of two-phase flow in a centrifugal pump with rotodynamic multi-impeller configurations," *African Journal of Advances in Engineering and Technology*, vol. 1, no. 2, pp. 5–27, 2025, https://hdl.handle.net/10520/ejc-aa_ajaet_v1_n2_a1.

[8] B. Blocken, "Computational Fluid Dynamics for urban physics: Importance, scales, possibilities, limitations and ten tips and tricks towards accurate and reliable simulations," *Building and Environment*, vol. 91, pp. 219–245, 2015, https://doi.org/10.1016/j.buildenv.2015.02.015

[9] H. K. Versteeg and W. Malalasekera, *An Introduction to Computational Fluid Dynamics: The Finite Volume Method*, 2nd ed. Harlow, UK: Pearson Education, 2007.

[10] A. K. Gupta, D. G. Lilley, and N. Syred, *Swirl Flows*. Tunbridge Wells, UK: Abacus Press, 1984, https://ui.adsabs.harvard.edu/abs/1984tw...book.....G/abstract.

[11] B. Xue, Y. Zhao, and C. Bi, "Investigation of flow field and pollutant particle distribution in the aquaculture tank for fish farming based on computational fluid dynamics," *Computers and Electronics in Agriculture*, vol. 200, p. 107243, 2022, https://doi.org/10.1016/j.compag.2022.107243.

[12] Z. Han, Z. Huang, S. Liu, D. Gan, S. Li, J. Hu, Y. Wang, and J. Zhang, "Optimization of thermal performance of vortex tube based on spiral nozzle and bulging belly structure," *Applied Thermal Engineering*, vol. 252, p. 126855, 2025, https://doi.org/10.1016/j.applthermaleng.2025.126855.

[13] A. Ouazzane and M. Barigou, "A comparative study of two flow conditioners and their efficacy to reduce asymmetric swirling flow effects on orifice meter performance," *Chemical Engineering Research and Design*, vol. 77, no. 6, pp. 495–504, 1999, https://doi.org/10.1205/026387699526728.

[14] A. de Lamotte, A. Delafosse, S. Calvo, and D. Toye, "Identifying dominant spatial and time characteristics of flow dynamics within free-surface baffled stirred tanks from CFD simulations," *Chemical Engineering Science*, vol. 192, pp. 128–142, 2018, https://doi.org/10.1016/j.ces.2018.07.024.

[15] M. Casey and T. Wintergerste, *ERCOFTAC Best Practice Guidelines for Industrial CFD*. ERCOFTAC Special Interest Group, 2020, http://oss.jishulink.com/caenet/forums/upload/2013/09/07/388/193287007808131.pdf

[16] W. L. Oberkampf and C. J. Roy, *Verification and Validation in Scientific Computing*. Cambridge, UK: Cambridge University Press, 2010, https://doi.org/10.1017/CBO9780511760396.

[17] J. P. Tullis, *Hydraulics of Pipelines: Pumps, Valves, Cavitation, Transients*. Hoboken, NJ, USA: Wiley, 1989. https://books.google.co.id/books?id=86P9PVgKXoEC.

[18] M. H. Chaudhry, *Applied Hydraulic Transients*, 3rd ed. New York, NY, USA: Springer, 2014, https://doi.org/10.1007/978-1-4614-8538-4.

[19] G. K. Batchelor, *An Introduction to Fluid Dynamics*. Cambridge, UK: Cambridge University Press, 2000. https://books.google.co.id/books?id=aXQgAwAAQBAJ.

[20] American Petroleum Institute, *Pressure-Relieving and Depressuring Systems*, API Standard 521, 6th ed. Washington, DC, USA, 2014, https://www.api.org/~/media/files/publications/whats%20new/521%20e6%20pa.pdf.

[21] American Petroleum Institute, *Design, Construction, Operation, Maintenance, and Inspection of Terminal and Tank Facilities*, API Standard 2610. Washington, DC, USA, 2020, https://www.api.org/-/media/apiwebsite/products-and-services/api-international-usage-and-deployment-report-2022.pdf.

[22] F. R. Menter, M. Kuntz, and R. Langtry, "Ten years of industrial experience with the SST turbulence model," *Turbulence, Heat and Mass Transfer*, vol. 4, pp. 625–632, 2003. https://www.researchgate.net/publication/228742295.

[23] S. B. Pope, *Turbulent Flows*. Cambridge, UK: Cambridge University Press, 2000, https://elmoukrie.com/wp-content/uploads/2022/04/pope-s.b.-turbulent-flows-cambridge-university-press-2000.pdf.

[24] P. J. Roache, *Verification and Validation in Computational Science and Engineering*. Albuquerque, NM, USA: Hermosa Publishers, 1998, https://pdfs.semanticscholar.org/0f3c/728bd0f17e45cce72bda2165707a0eb9e03b.pdf/1000.

[25] R. Hisamatsu, Y. Yamaguchi, C. A. Riveros-Jerez, and T. Utsunomiya, "Experimental and numerical investigation of the inlet effect on the dynamics of a water intake pipe," in *Proc. Int. Conf. Offshore Mechanics and Arctic Engineering*, vol. 87844, p. V006T08A047, 2024, https://doi.org/10.1115/OMAE2024-124537.

[26] W. Ma, C. Zhang, C. Pan, M. Lu, J. Li, J. Ma, and K. Qin, "CFD-based flow simulation and optimization of horizontal tube sedimentation tanks (HTST)," *Process Safety and Environmental Protection*, vol. 179, p. 107287, 2025, https://doi.org/10.1016/j.psep.2025.107287.

[27] Z. Wang, D. Liu, B. Ji, and X. Luo, "Multiscale investigation of cavitation surge characteristics in the swirling flow using Eulerian-Lagrangian method," *Ultrasonics Sonochemistry*, vol. 94, p. 107466, 2025, https://doi.org/10.1016/j.ultsonch.2025.107466.

[28] X. Li, R. Zhou, H. Wang, X. Yan, and H. Zhang, "Enhanced mixing and conditioning by bidirectional swirling flow: A numerical–experimental approach," *Powder Technology*, p. 121576, 2025, https://doi.org/10.1016/j.powtec.2025.121576.

[29] H. Bie,Y. Li, R. Zhang, L. Xue, G. Liu, Z. Hao, "Effect of swirl flow on bubble motion and spatial distribution in CO_2 capture processes," *Chemical Engineering Journal*, vol. 480, p. 148341, 2024, https://doi.org/10.1016/j.cej.2023.148341.

[30] B. E. Launder and D. B. Spalding, "The numerical computation of turbulent flows," *Numerical Prediction of Flow, Heat Transfer, Turbulence and Combustion*, vol. 3, no. 2, pp. 96–116, 1983, https://doi.org/10.1016/B978-0-08-030937-8.50016-7.

[31] S. O. Effiom, F. I. Abam, A. T. Assam, P.-C. O. Effiom, O. C. Onochie, and O. I. Inah, "Shielding offshore gas turbines: A validated CFD approach to multistage inlet-air filtration," *Saudi Journal of Engineering and Technology*, vol. 11, no. 1, pp. 31–43, 2026, https://doi.org/10.36348/sjet.2026.v11i01.003.

[32] J. Kim and P. Moin, "Application of a fractional-step method to incompressible Navier–Stokes equations," *Journal of Computational Physics*, vol. 59, no. 2, pp. 308–323, 1985, https://doi.org/10.1016/0021-9991(85)90148-2.

[33] R. I. Issa, "Solution of the implicitly discretised fluid flow equations by operator-splitting," *Journal of Computational Physics*, vol. 62, no. 1, pp. 40–65, 1986, https://doi.org/10.1016/0021-9991(86)90099-9.

[34] J. H. Ferziger and M. Perić, *Computational Methods for Fluid Dynamics*, 3rd ed. Berlin, Germany: Springer, 2002. https://link.springer.com/book/10.1007/978-3-319-99693-6.

[35] E. M. Sparrow, J. M. Gorman, J. P. Abraham, and W. Minkowycz, "Chapter One – Validation of turbulence models for numerical simulation of fluid flow and convective heat transfer," *Advances in Heat Transfer*, vol. 49, pp. 1–35, 2017, https://doi.org/10.1016/bs.aiht.2017.09.002.

[36] S. O. Effiom, F. I. Abam, and B. N. Nwankwojike, "Turbomachinery design modification and analysis of the axial turbine of an aeroderivative gas turbine," *Nigerian Journal of Technological Research*, vol. 13, no. 2, pp. 31–38, 2018, https://doi.org/10.4314/njtr.v13i2.5.